PHYSICAL REVIEW B **93**, 195106 (2016)

Electronic structures of transition metal dipnictides XPn_2 (X = Ta, Nb; Pn = P, As, Sb)

Chenchao Xu,[1] Jia Chen,[2] Guo-Xiang Zhi,[1] Yuke Li,[2] Jianhui Dai,[2,*] and Chao Cao[2,†]
[1]*Department of Physics, Zhejiang University, Hangzhou 310036, China*
[2]*Condensed Matter Group, Department of Physics, Hangzhou Normal University, Hangzhou 310036, China*

(Received 7 February 2016; revised manuscript received 6 April 2016; published 3 May 2016)

The electronic structures and topological properties of transition metal dipnictides XPn_2 (X = Ta, Nb; Pn = P, As, Sb) have been systematically studied using first-principles calculations. In addition to small bulk Fermi surfaces, the band anticrossing features near the Fermi level can be identified from band structures without spin-orbit coupling, leading to nodal lines in all these compounds. Inclusion of spin-orbit coupling gaps out these nodal lines, leaving only a pair of disentangled electron/hole bands crossing the Fermi level. Therefore, the low-energy physics can be in general captured by the corresponding two-band model with several isolated small Fermi pockets. Detailed analysis of the Fermi surfaces suggests that the arsenides and $NbSb_2$ are nearly compensated semimetals while the phosphorides and $TaSb_2$ are not. Based on the calculated band parities, the electron and hole bands are found to be weakly topological nontrivial, giving rise to surface states. As an example, we presented the surface-direction-dependent band structure of the surfaces states in $TaSb_2$.

DOI: 10.1103/PhysRevB.93.195106

I. INTRODUCTION

Over the past two decades, an exciting development in the condensed matter physics community has revolutionized the classification of materials. In addition to the traditional conductors, insulators, and semiconductors, it has been discovered that symmetries of the crystal may lead to more delicate differences, giving rise to topologically trivial and nontrivial phases [1–3]. The difference between the topological insulators (TI) and normal insulators (NI) lies at their surfaces, the respective interface with a NI, vacuum. The topological change across the interface dictates the existence of a symmetry-protected metallic surface state for TI, leading to distinct magnetoelectronic responses. For instance, the metallic surface state will result in a resistivity plateau in transport measurement, which is regarded as the hallmark of TI in many cases [4–6].

The study of topological materials was advanced with the discovery of three-dimensional Weyl semimetals. A Weyl semimetal has separated right- and left-handed nodal points in momentum space breaking, the $\mathcal{TP}$ symmetry, and can thus be realized either in centrosymmetric topological materials without the time-reversal $\mathcal{T}$ symmetry [7,8] or in noncentrosymmetric topological materials without the space inversion or parity symmetry $\mathcal{P}$ [9–11]. The presence of the left and right Weyl points will lead to other intriguing phenomena, including formation of disconnected Fermi arcs [7,8]. In particular, because of the chiral anomaly of relativistic Weyl fermions generated by coupling to the gauge potential, the negative magnetoresistance with unusual dependence on the electric and magnetic fields may occur in these materials [12,13].

More recently, a class of transition metal dipnictides has been experimentally synthesized and characterized [14–19]. All these compounds were reported to exhibit high mobilities and extremely large positive magnetoresistances (MRs) when the applied field is perpendicular to the current direction, similar to previously known Weyl semimetals. Another common feature of these compounds is the field-induced metal-insulator transition, which in some cases results in a very clear resistivity plateau at low temperatures [15,16]. Interestingly, negative longitudinal MRs when the applied field is parallel to the current direction were reported in $TaSb_2$ [15] and $TaAs_2$ [18]. All these features imply the rich physics beyond the known TIs and Weyl semimetals. On the one hand, the large positive MR is mostly attributed to the semiclassical effect of electron-hole compensation [17,19], while the field-induced metal-insulator transition may be associated with the gap opening in quasi-two-dimensional systems with low carrier density and high mobility [15]. On the other hand, the field-induced resistivity plateau and negative MR should have some topological origins, although their appearances are seemingly materials dependent. So far limited band structure information has been occasionally presented together with the experimental studies [14,15,17,18], but the reported results are far from complete and a thorough comparison for band structures of all these materials is obviously lacking. Therefore, a systematic study of electronic structures of this class of materials is urgently demanded.

In this article, we present our latest first-principles results on these compounds. Our results show a number of common features of their band structures as well as several important distinctions. In particular, we show that the bulk electronic states of these materials can be regarded as two-band system with both electron and hole contributions. The phosphrides (TaP_2 and NbP_2) are highly uncompensated with many more holes than electrons, while $TaSb_2$ has slightly more electrons than holes. The rest of the arsenides and $NbSb_2$ are nearly compensated. Moreover, both the electron and hole bands are weakly topological in all these materials, leading to protected surface states of these compounds.

II. METHOD

The calculations were performed with density functional theory (DFT) as implemented in the VIENNA AB INITIO SIMULATION PACKAGE (VASP) [20,21]. A plane-wave basis up

---

[*] daijh@hznu.edu.cn
[†] ccao@hznu.edu.cn

TABLE I. Optimized geometry parameters of XPn_2 compounds. β is the angle formed by **a** and **c** lattice vectors. The numbers in the parenthesis are experimental values for comparison purposes, from Refs. [14–17,26] for NbP_2, $NbAs_2$, $NbSb_2$, TaP_2, $TaAs_2$, and $TaSb_2$, respectively; whereas the internal coordinates for antimonides and $TaAs_2$ are from Refs. [27] and [18], respectively.

	NbP_2 [26]	$NbAs_2$ [16]	$NbSb_2$ [14]	TaP_2 [26]	$TaAs_2$ [17]	$TaSb_2$ [15]
a (Å)	8.902 (8.872)	9.454 (9.354)	10.359 (10.233)	8.892 (8.861)	9.441 (9.329)	10.356 (10.223)
b (Å)	3.290 (3.266)	3.418 (3.381)	3.676 (3.630)	3.290 (3.268)	3.422 (3.385)	3.697 (3.645)
c (Å)	7.584 (7.510)	7.884 (7.795)	8.423 (8.328)	7.543 (7.488)	7.843 (7.753)	8.385 (8.292)
β	118.97 (119.10)	119.40	120.04 (120.04)	119.23 (119.31)	119.70 (119.70)	120.52 (120.39)
x_X	0.1598 (0.154)	0.1569 (0.154)	0.1516 (0.157)	0.1601 (0.154)	0.1569 (0.157)	0.1504 (0.16)
z_X	0.2007 (0.200)	0.1961 (0.196)	0.1902 (0.196)	0.2002 (0.200)	0.1954 (0.196)	0.1883 (0.20)
$x_{Pn,I}$	0.4029 (0.399)	0.4050 (0.399)	0.4050 (0.404)	0.4037 (0.399)	0.4055 (0.406)	0.4051 (0.40)
$z_{Pn,I}$	0.1000 (0.112)	0.1065 (0.107)	0.1116 (0.196)	0.1012 (0.112)	0.1075 (0.107)	0.1125 (0.11)
$x_{Pn,II}$	0.1334 (0.143)	0.1414 (0.140)	0.1489 (0.142)	0.1331 (0.143)	0.1406 (0.139)	0.1486 (0.14)
$z_{Pn,II}$	0.5258 (0.531)	0.5286 (0.526)	0.5358 (0.527)	0.5251 (0.531)	0.5275 (0.526)	0.5351 (0.53)

to 400 eV was employed in the calculations. Throughout the calculation, the Perdew, Burke, and Ernzerhof parametrization (PBE) of generalized gradient approximation to the exchange correlation functional was used [22]. The crystal structure was fully optimized using the conventional cell with $4 \times 12 \times 5$ Γ-centered K mesh until the force on each atom was less than 1 meV/Å and internal stress was less than 0.1 kbar. The subsequent electronic structure calculations were then performed with primitive cell and a $8 \times 8 \times 5$ Γ-centered K mesh.

The topological indices $\mathcal{Z}_2$ were calculated using the parity-check method proposed by Fu *et al.* [23]. The DFT band structures were fitted to a tight-binding (TB) model Hamiltonian using the maximally localized Wannier function (MLWF) method [24] with Ta-5d and Sb-5p orbitals. The Fermi surfaces were then obtained by extrapolating the TB Hamiltonian on a $100 \times 100 \times 100$ K mesh; and the surface states were calculated using the TB Hamiltonian by calculating the surface Green's function [25].

III. RESULTS AND DISCUSSION

A. Crystal structure and Brillouin zone

First of all, we show the optimized geometry parameters of XPn_2 compounds with spin-orbit coupling (SOC) effect considered (Table I) [28]. All compounds share the same centrosymmetric base-centered monoclinic structure with space group $C_{12/m1}$, as shown in Fig. 1(a). The calculated lattice constants as well as the atomic coordinates are within 5% error bar compared to the experimental values, manifesting the validity of our calculations. Since the conventional unit cell consists of 2 primitive cells, the primitive Brillouine zone (BZ) is twice large as the conventional BZ. The BZ for the primitive cell, as well as the definition of high-symmetry points, is illustrated in Fig. 1(b).

B. Bulk band structure and DOS

With the optimized structure, we calculated the bulk band structures without the SOC effect (Fig. 2). The overall band structures of these compounds resemble each other, while the systematic changes can be traced. For all the compounds, there are one electron band and one hole band which cross the Fermi level E_F, suggesting the two-band feature and coexistence of electron/hole carriers in these materials. In addition, two anticrossing features can always be identified within 0.2 eV of the Fermi level E_F as indicated by the blue circles. These band inversion properties can be verified with symmetry analysis for the states near the K-points. By explicitly calculating the coordinates of the nodal K-points for the $TaSb_2$ compound, we have found that these band-crossing K-points form nodal lines, consistent with the general argument posed by Weng *et al.* [29,30]. For phosphorides, the two anticrossings are energetically separated and far from E_F. They are closer in arsenides, and eventually become energetically almost degenerate and very close to E_F in antimonides. Furthermore, the direct gap at Z from the electron to hole band is increased from a few meVs in NbP_2 to ~400 meV $TaSb_2$, reflecting the increase of atom sizes and the bond lengths. Similar changes can also be seen around F, F_1, and in between L and I. Thus, more anticrossing features can be identified in either arsenides or antimonides, as indicated by the green circles in Figs. 2(b), 2(c), 2(e), and 2(f). It is also interesting to notice that the anticrossing features from L to I are highly asymmetric when present, different from all others.

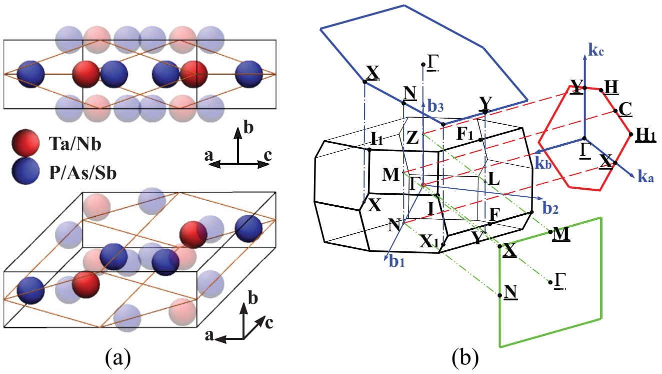

(a) (b)

FIG. 1. (a) Conventional (the larger black box) and primitive (the smaller orange box) cells of XPn_2. Transparent atoms only appears in the conventional cell. (b) Primitive Brillouin zone (BZ), the reciprocal lattice vectors of conventional BZ (k_a, k_b, and k_c), the BZ of conventional [100] (green solid lines), [010] surface (red solid lines), [001] surface (blue solid lines), and their respective high symmetry points.

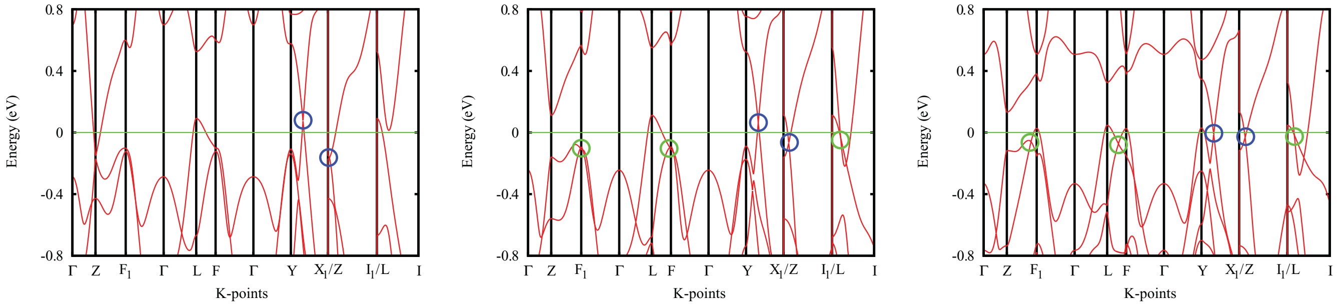

(a) NbP2 (b) NbAs2 (c) NbSb2

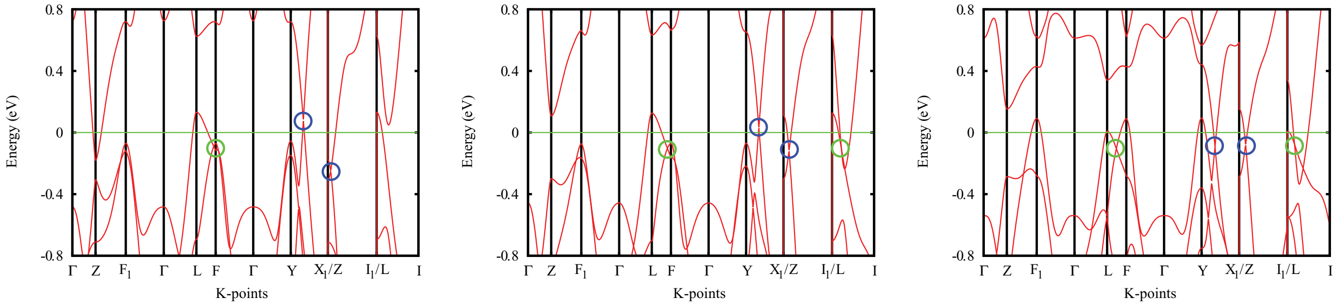

(d) TaP2 (e) TaAs2 (f) TaSb2

FIG. 2. Bulk band structure of XPn_2 calculated without SOC (reproduced with MLWF-fitted TB Hamiltonians). The circles indicates anticrossing features within $E_F \pm 200$ meV range. The Fermi energy is aligned at 0. The blue circled features are present in all compounds, while the green circled features are not.

Once the SOC effect is taken into consideration (Fig. 3), all the above nodal lines become gapped, leaving us a pair of fully gapped hole band and electron band. Furthermore, these bands are also completely separated from all other bands in the whole BZ. Therefore, $\mathcal{Z}_2$ invariants can be calculated for each of these bands. Apart from the gap of nodal lines, some other interesting features can be identified in Fig. 3. First, the size of the SOC splitting roughly follows the order of Nb < Ta and P < As < Sb, consistent with normal expectation. Second, the gapped states close to Z form two very small electron pockets for arsenides and antimonides, while the gapped states close to Y form two small hole pockets for NbP_2 and $NbAs_2$. The

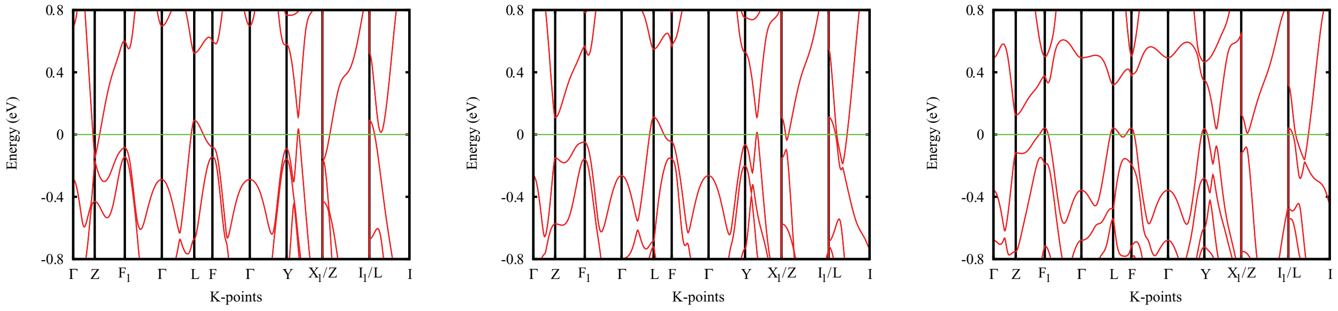

(a) NbP2 (b) NbAs2 (c) NbSb2

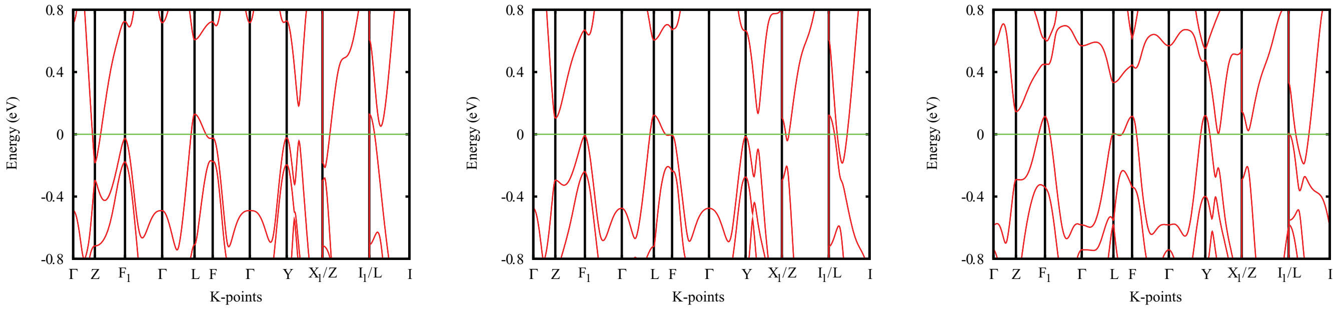

(d) TaP2 (e) TaAs2 (f) TaSb2

FIG. 3. Bulk band structure of XPn_2 calculated with SOC. The Fermi energy is aligned at 0.

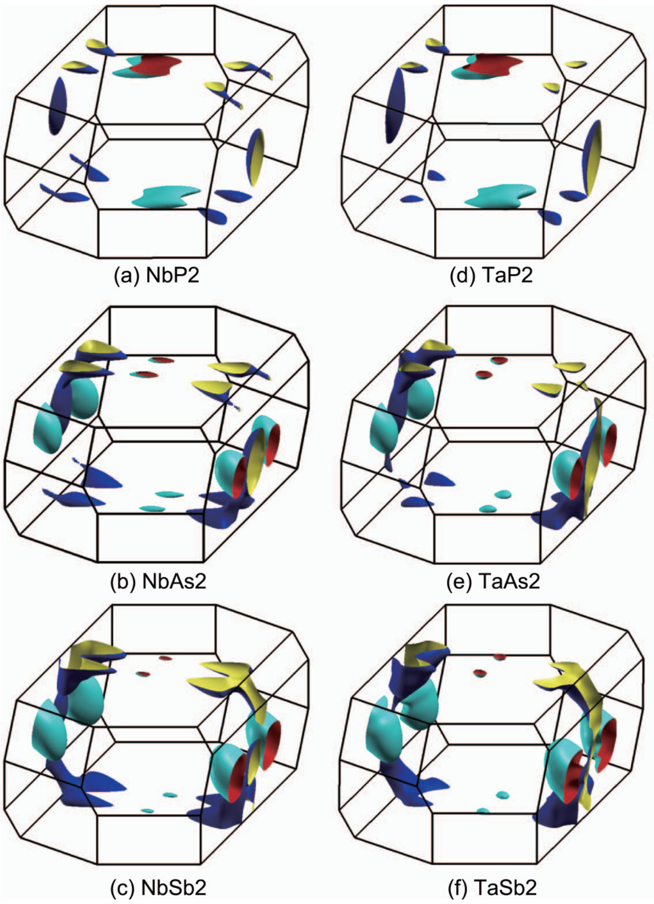

FIG. 4. Fermi surfaces of XPn_2 calculated with SOC (using MLWF-fitted TB Hamiltonians). In all compounds, there are 3 isolated pockets, including 2 large ones and 1 small one.

formation of these small closed pockets can also be evidenced from the Fermi surface (FS) plot of these compounds (Fig. 4). The density of states (DOS) at the Fermi level $n(E_F)$ are evaluated to be 0.099 (NbP_2), 0.546 ($NbAs_2$), 1.084 ($NbSb_2$), 0.115 (TaP_2), 0.583 ($TaAs_2$), and 0.803 ($TaSb_2$) states per unit cell per eV, respectively. The systematic increase of $n(E_F)$ from phosphrides to antimonides is consistent with the increase of FS area and proportional to the carrier density in these compounds and the metallicity thereafter.

TABLE II. Parities of bands at time-reversal invariant momenta (TRIM) Γ: (0,0,0), N: $(\pi, 0, 0)$, N′: $(0, \pi, 0)$, Y: $(\pi, \pi, 0)$, Z: $(0, 0, \pi)$, M: $(\pi, 0, \pi)$, M′: $(0, \pi, \pi)$ and L: (π, π, π). Π_n is the multiplication of the parities for bands 1 to n. The highest occupied band at each TRIM is indicated with °.

	XP_2				XAs_2				XSb_2			
	Π_{20}	Π_{21}	Π_{22}	Π_{23}	Π_{20}	Π_{21}	Π_{22}	Π_{23}	Π_{20}	Π_{21}	Π_{22}	Π_{23}
Γ	+	− °	+	−	+	− °	+	−	+	− °	+	−
N	+	+ °	+	+	+	+ °	+	−	+	+ °	+	−
N′	+	+ °	+	+	+	+ °	+	−	+	+ °	+	−
Y	+	+ °	+	−	+	+ °	+	−	+ °	+	+	−
Z	+	−	− °	+	+	− °	−	+	+	− °	−	+
M	+	− °	−	−	+	− °	−	−	+	− °	−	−
M′	+	− °	−	−	+	− °	−	−	+	− °	−	−
L	+ °	+	−	+	+ °	+	−	−	+ °	+	−	−

Closer examination of the FS plots reveals further details of these compounds. From phosphorides to antimonides, the increase of $n(E_F)$ is due to increase of both hole FS (blue/green sheets) and electron FS (cyan/red sheets) (Fig. 4). We can also identify the electron/hole DOS contribution by evaluating the second derivative of band energy $m_{\alpha\beta} = d^2\epsilon_{\mathbf{k}}/dk_\alpha dk_\beta$ for all bands crossing the Fermi level. It has been proposed that the large MR observed was due to nearly compensated electron/hole density [16,17]. As the current direction is usually aligned along the **b** axis, we classified the contribution according to m_{bb}. The electron/hole DOS ratio for these compounds are 1:2.4 (NbP_2), 1:1.13 ($NbAs_2$), 1.05:1 ($NbSb_2$), 1:1.9 (TaP_2), 1:1.16($TaAs_2$), and 1.25:1 ($TaSb_2$), respectively. Thus, the phosphrides are highly uncompensated with many more holes than electrons, and $TaSb_2$ has slightly more electrons than holes, while all other compounds are nearly compensated. Although such classification is very crude indeed, it agrees with previous experimental results [15–17,19].

C. $\mathcal{Z}_2$ invariants

Since the structure has an inversion center, the topological indices can be easily calculated by examining the parities of occupied bands at the time-reversal invariant momenta (TRIM) [23]. Noticing that both the 21st and 22nd bands cross the Fermi level E_F, we calculated four sets of $\mathcal{Z}_2$ numbers Π_{20}, Π_{21}, Π_{22}, and Π_{23}, where Π_n is the multiplication of the parities for bands 1 to n. The Π_{20}, Π_{21}, and Π_{22} are exactly the same for all these compounds, and Π_{20} for all TRIMs are +1, suggesting that the fully occupied

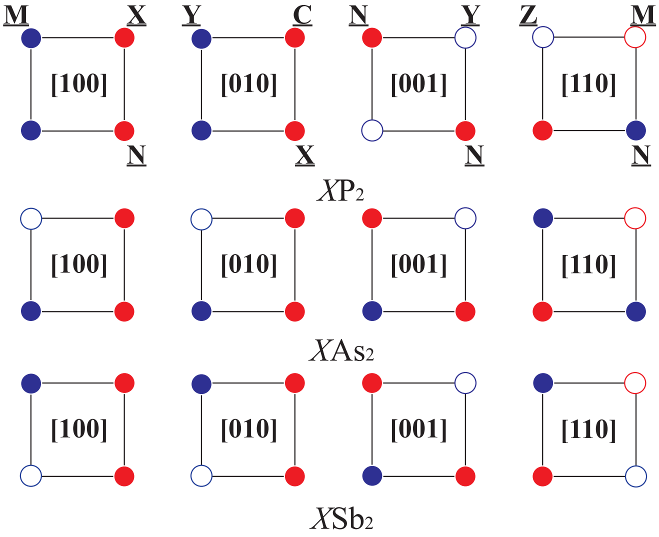

FIG. 5. Illustration of possible surface states. The rows from top to bottom are phosphorides, arsenides, and antimonides, respectively. The bottom left corner of each panel is $\underline{\Gamma}$, and the surface indices are illustrated at the center of the panel. The blue/red circles represent +/− polarizations, respectively; and open circles indicate overwhelming bulk states due to occupations. Topological surface states can be present between solid circles with different colors.

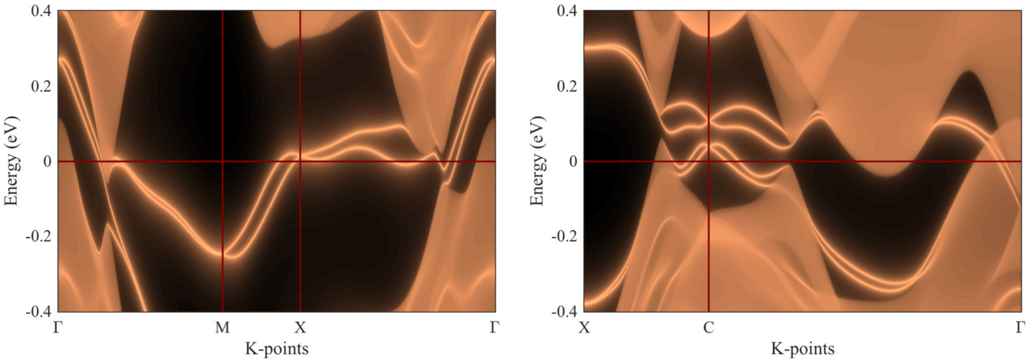

(a) [100] surface (b) [010] surface

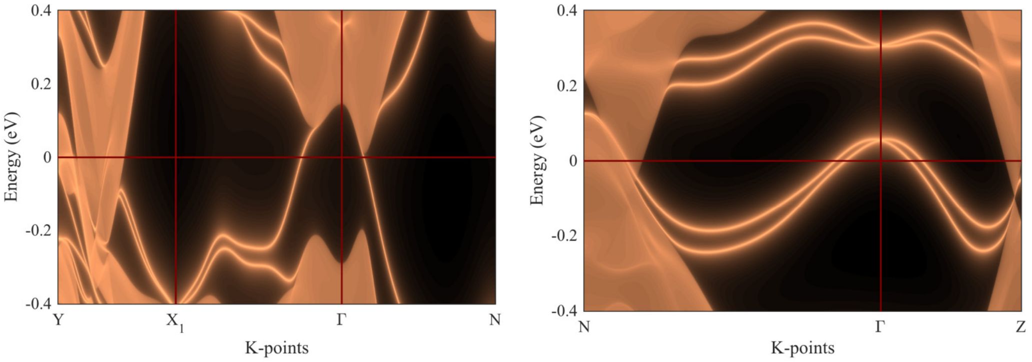

(c) [001] surface (d) [110] surface

FIG. 6. Surface states of $TaSb_2$. The surface direction is labeled in the conventional cell; thus the [110] surface is indeed the [100] surface of the primitive cell.

bands are topologically trivial. Although the occupations at each TRIM vary with respect to the pnictogen, the $\mathcal{Z}_2$ classification can be determined to be (0; 111) for all these compounds. Nevertheless, the emergence of surface state of weakly topological material is not universal and depends on the details of TRIMs of the specific surface. We shall clarify this in the next section. Interestingly, Π_{23}s of both arsenides and antimonides correspond to $\mathcal{Z}_2$ classification (1; 111) and are topologically strong. This may lead to other topological insulators in similar compounds.

D. Surface states

In order to calculate the surface state in these compounds, we first identify the two-dimensional (2D) BZs for certain important surfaces. Since the conventional cell is constructed from the primitive cell using $\mathbf{a} = \mathbf{a}' + \mathbf{b}'$, $\mathbf{b} = -\mathbf{a}' + \mathbf{b}'$ and $\mathbf{c} = \mathbf{c}'$; the [100] surface of the primitive cell is therefore [110] surface of the conventional cell. To avoid confusion, we label the surfaces using conventional cell index from now on. The 2D BZs of the [100], [010], and [001] surfaces are illustrated in Fig. 1(b).

As we have identified previously, the electron polarizations at each TRIM are exactly the same for all these materials, in spite of the different occupations involved. Therefore, the presence of the metallic surface state depends on two factors: the polarization at the TRIMs of the specific surface and the occupations at those TRIMs. The latter is not relevant in insulators since the universal bulk gap ensures the occupations at all TRIMs to be the same. It is not the case in topological metals because it may introduce metallic bulk state. Indeed, there are 42 valence electrons in the primitive cell, corresponding to 21 filled bands if the compound is an insulator. Therefore, if any of the two bulk TRIM occupations corresponding to the same surface TRIM is different from 21, the bulk state would overwhelm around the specific surface TRIM, suppressing the emergence of the surface state near it. Away from this TRIM, metallic surface states can still emerge, but will not be symmetry protected. With the above statement in mind, we can identify symmetry-protected surface states in these materials as illustrated in Fig. 5. The surface states can be present between two TRIMs only if both TRIMs are solid and filled with opposite colors. We demonstrate the surface states of $TaSb_2$ in detail in Fig. 6.

IV. CONCLUSION

In conclusion, we have performed a systematic study of the electronic structures and topological properties of transition metal dipnictides XPn_2 (X = Ta, Nb; Pn = P, As, Sb) using first-principles calculations. Nodal line features can be identified in these compounds, and the inclusion of spin-orbit coupling gaps out all the anticrossing features. Small electron (hole) pockets due to the gapped nodal states can be identified in arsenides and antimonides (NbP_2 and $NbAs_2$), respectively. The DOS at E_F systematically increases in the order of phosphorides < arsenides < antimonides. Furthermore, $NbAs_2$, $NbSb_2$, and $TaAs_2$ are nearly compensated semimetals; the phosphorides have many more holes than electrons; while the $TaSb_2$ has slightly more electrons than holes. By calculating the band parities, we found both the electron and hole bands are weakly topological and thus give rise to surfaces states, although these states are not as robust as the ones emerging from strongly topological insulators and depend on details including the electron polarizations at TRIMs and the electron occupations.

Note added. Recently, we became aware of the work by Shen *et al.* [31]. They have also observed negative MR in NbAs_2, and their band structure results are in good agreement with ours. We notice that the three Fermi pockets in their calculation are due to the folded BZ for the conventional cell instead of the primitive one. The F_c frequency from their experiment may be due to the two small pockets close to the Z point in our calculation, which become indistinguishable because of the identical shapes and small sizes.

ACKNOWLEDGMENTS

This work has been supported by the 973 Project (No. 2014CB648400), the NSFC (No. 11274006, No. 11474082, and No. 11274267), and the Zhejiang Provincial Natural Science Foundation (No. LR12A04003 and No. LZ13A040001). All calculations were performed at the High Performance Computing Center of Hangzhou Normal University College of Science.

---

[1] L. Fu, C. L. Kane, and E. J. Mele, Phys. Rev. Lett. **98**, 106803 (2007).
[2] M. Z. Hasan and C. L. Kane, Rev. Mod. Phys. **82**, 3045 (2010).
[3] X.-L. Qi and S.-C. Zhang, Rev. Mod. Phys. **83**, 1057 (2011).
[4] Z. Ren, A. A. Taskin, S. Sasaki, K. Segawa, and Y. Ando, Phys. Rev. B **82**, 241306 (2010).
[5] S. Jia, H. Beidenkopf, I. Drozdov, M. K. Fuccillo, J. Seo, J. Xiong, N. P. Ong, A. Yazdani, and R. J. Cava, Phys. Rev. B **86**, 165119 (2012).
[6] D. J. Kim, J. Xia, and Z. Fisk, Nat. Mater. **13**, 466 (2014).
[7] X. Wan, A. M. Turner, A. Vishwanath, and S. Y. Savrasov, Phys. Rev. B **83**, 205101 (2011).
[8] G. Xu, H. Weng, Z. Wang, X. Dai, and Z. Fang, Phys. Rev. Lett. **107**, 186806 (2011).
[9] H. Weng, C. Fang, Z. Fang, B. A. Bernevig, and X. Dai, Phys. Rev. X **5**, 011029 (2015).
[10] B. Q. Lv, H. M. Weng, B. B. Fu, X. P. Wang, H. Miao, J. Ma, P. Richard, X. C. Huang, L. X. Zhao, G. F. Chen *et al.*, Phys. Rev. X **5**, 031013 (2015).
[11] B. Q. Lv, S. Muff, T. Qian, Z. D. Song, S. M. Nie, N. Xu, P. Richard, C. E. Matt, N. C. Plumb, L. X. Zhao *et al.*, Phys. Rev. Lett. **115**, 217601 (2015).
[12] D. T. Son and B. Z. Spivak, Phys. Rev. B **88**, 104412 (2013).
[13] X. Huang, L. Zhao, Y. Long, P. Wang, D. Chen, Z. Yang, H. Liang, M. Xue, H. Weng, Z. Fang *et al.*, Phys. Rev. X **5**, 031023 (2015).
[14] K. Wang, D. Graf, L. Li, L. Wang, and C. Petrovic, Sci. Rep. **4**, 7328 (2014.
[15] Y. Li, L. Li, J. Wang, T. Wang, X. Xu, C. Xi, C. Cao, and J. Dai, arXiv:1601.02062.
[16] Y.-Y. Wang, Q.-H. Yu, and T.-L. Xia, arXiv:1601.04239.
[17] D. Wu, J. Liao, W. Yi, X. Wang, P. Li, H. Weng, Y. Shi, Y. Li, J. Luo, X. Dai *et al.*, Appl. Phys. Lett. **108**, 042105 (2016).
[18] Y. Luo, R. D. McDonald, P. F. S. Rosa, B. Scott, N. Wakeham, N. J. Ghimire, E. D. Bauer, J. D. Thompson, and F. Ronning, arXiv:1601.05524.
[19] Z. Yuan, H. Lu, Y. Liu, J. Wang, and S. Jia, arXiv:1601.06482.
[20] G. Kresse and J. Hafner, Phys. Rev. B **47**, 558 (1993).
[21] G. Kresse and D. Joubert, Phys. Rev. B **59**, 1758 (1999).
[22] J. P. Perdew, K. Burke, and M. Ernzerhof, Phys. Rev. Lett. **77**, 3865 (1996).
[23] L. Fu and C. L. Kane, Phys. Rev. B **76**, 045302 (2007).
[24] I. Souza, N. Marzari, and D. Vanderbilt, Phys. Rev. B **65**, 035109 (2001).
[25] M. P. L. Sancho, J. M. L. Sancho, J. M. L. Sancho, and J. Rubio, J. Phys. F **15**, 851 (1985).
[26] S. Rundqvist, Nature (London) **211**, 847 (1966).
[27] S. Furuseth and A. Kjekshus, Nature (London) **203**, 512 (1964).
[28] The geometry parameters obtained without SOC differ by less than 1% compared to those obtained with SOC.
[29] H. Weng, Y. Liang, Q. Xu, R. Yu, Z. Fang, X. Dai, and Y. Kawazoe, Phys. Rev. B **92**, 045108 (2015).
[30] R. Yu, H. Weng, Z. Fang, X. Dai, and X. Hu, Phys. Rev. Lett. **115**, 036807 (2015).
[31] B. Shen, X. Deng, G. Kotliar, and N. Ni, arXiv:1602.01795.